HARRAN ÜNİVERSİTESİ MÜHENDİSLİK DERGİSİ

HARRAN UNIVERSITY JOURNAL of ENGINEERING

e-ISSN: 2528-8733 (ONLINE)
URL: https://dergipark.org.tr/tr/pub/humder

Gama Işını Zırhlaması için Düşük-Z ve Yüksek-Z Malzemelerde Foton Etkileşim Kesitlerinin Baskınlık Grafikleriyle Sistematik Karşılaştırılması

Systematic Comparison of Photon Interaction Cross-Sections from Low-Z to High-Z Materials Using Dominance Graphs for Gamma-Ray Shielding

Yazar(lar) (Author(s)): İlker Can ÇELİK[1]

[1]ORCID ID: 0000-0002-2320-6584

Bu makaleye şu şekilde atıfta bulunabilirsiniz (To cite to this article): Celik I.C., "Systematic Comparison of Photon Interaction Cross-Sections from Low-Z to High-Z Materials Using Dominance Graphs for Gamma-Ray Shielding", Harran University Journal of Engineering, 11(1): 69-92, (2026).

Erişim linki (To link to this article): 10.46578/humder.1906695

Harran Üniversitesi Mühendislik Dergisi

Harran University Journal of Engineering

https://dergipark.org.tr/tr/pub/humder

Araştırma Makalesi (Research Article)

Gama Işını Zırhlaması için Düşük-Z ve Yüksek-Z Malzemelerde Foton Etkileşim Kesitlerinin Baskınlık Grafikleriyle Sistematik Karşılaştırılması

Ilker Can CELIK*,[1]

[1]Fizik Bolumu, Fen Edebiyat Fakultesi, Harran Universitesi, Sanliurfa, Turkiye

Makale Bilgisi

Başvuru: 10/03/2026
Düzeltme: 24/03/2026
Kabul: 30/03/2026
Yayınlanma: 31/03/2026

Alıntı

Celik I.C., "Gama Işını Zırhlaması için Düşük-Z ve Yüksek-Z Malzemelerde Foton Etkileşim Kesitlerinin Baskınlık Grafikleriyle Sistematik Karşılaştırılması", Harran Üniversitesi Mühendislik Dergisi, 11(1): 69-92, (2026).

Özet

Bu çalışma, gama ışını zırhlama performansının farklı enerji bölgelerinde daha anlaşılır yorumlanabilmesi için, düşük-Z'den yüksek-Z'ye uzanan temsili malzemeler için foton etkileşim tesir kesitlerinin sistematik ve karşılaştırmalı bir analizini sunmaktadır. XCOM gibi veri tabanlarında kapsamlı tesir kesiti verileri bulunmasına rağmen, mevcut çalışmaların çoğu tekil malzemelere veya tablosal verilere odaklanmakta ve geniş enerji aralıklarında foton etkileşim mekanizmalarının göreli baskınlığına sınırlı bilgi sunmaktadır. Bu çalışmada, fotoelektrik soğurma, Compton saçılması ve çift oluşumu dahil toplam ve kısmi zayıflatma katsayıları, seçilen malzemeler (B, Al, Si, Cu, W, Pb, su ve hava) için 1 keV–20 MeV aralığında XCOM veri tabanından elde edilmiştir. Bu malzemeler, nükleer, tıbbi, havacılık ve endüstriyel uygulamalarda yaygın kullanılan zırhlama ve yapısal malzemeleri temsil etmektedir. Farklı etkileşim mekanizmalarının göreli katkılarını karşılaştırmak için baskınlık temelli bir görselleştirme yaklaşımı geliştirilmiştir. Sonuçlar, foton enerjisi ve atom numarasına bağlı sistematik geçişler olduğunu göstermektedir. Bu yaklaşım, foton-madde etkileşimlerinin daha iyi anlaşılmasını sağlamakta ve özellikle çok katmanlı veya kompozit zırhlama sistemlerinde malzeme seçimini desteklemektedir.

Anahtar Kelimeler: *Gama ışını zayıflatma, Zırhlama baskınlık görselleştirmesi, XCOM veritabanı, Fotoelektrik etki, Compton saçılması, Çift oluşumu, Radyasyon zırhlaması.*

Systematic Comparison of Photon Interaction Cross-Sections from Low-Z to High-Z Materials Using Dominance Graphs for Gamma-Ray Shielding

Article Information

Received: 10/03/2026
Revised: 24/03/2026
Accepted: 30/03/2026
Published: 31/03/2026

Citation

Celik I.C., "Systematic Comparison of Photon Interaction Cross-Sections from Low-Z to High-Z Materials Using Dominance Graphs for Gamma-Ray Shielding", Harran University Journal of Engineering, 11(1): 69-92, (2026).

Abstract

This study presents a systematic and comparative analysis of photon interaction cross-sections for representative materials spanning low-Z to high-Z regimes to improve the interpretability of gamma-ray shielding performance across different energy domains. Although extensive cross-sectional data are available in databases such as XCOM, most studies focus on individual materials or tabulated values and provide limited insight into the relative dominance of photon interaction mechanisms over wide energy ranges. In this work, total and partial attenuation coefficients, including photoelectric absorption, Compton scattering, and pair production, were obtained from the XCOM database for selected materials (B, Al, Si, Cu, W, Pb, water, and air) over 1 keV–20 MeV. These materials represent commonly used shielding and structural materials in nuclear, medical, aerospace, and industrial applications. A dominance-based visualization approach was developed to compare the relative contributions of photon interaction mechanisms. The results reveal systematic transitions between interaction regimes with photon energy and atomic number and support preliminary material selection for multilayer or composite gamma-ray shielding systems.

Keywords: *Gamma-ray attenuation, Shielding dominance visualization, XCOM database, Photoelectric effect, Compton scattering, Pair production, Radiation shielding.*

*İletişim yazarı, e-mail: ilkercan0066@harran.edu.tr
*Corresponding author, e-mail: ilkercan0066@harran.edu.tr
DOI: 10.46578/humder.1906695

1. INTRODUCTION

Gamma radiation, one of the most penetrating forms of ionizing radiation, poses significant risks in nuclear power, medical imaging, aerospace, and industrial applications. Effective shielding is essential for protecting personnel and equipment and for complying with safety regulations from organizations such as ICRP [1], IAEA [2], and NRC [3]. Its applications include nuclear reactors, radiotherapy, diagnostic imaging, spacecraft, and industrial radiography. For example, Co-60 therapy and PET/SPECT imaging require proper shielding for both operators and patients. Space missions face gamma-ray hazards from cosmic rays, necessitating lightweight shielding materials such as water and polyethylene. In industry, gamma rays are used in non-destructive testing and food sterilization, while homeland security relies on shielding to detect and contain radiological threats. These challenges have driven innovations in shielding materials, including composites, nanomaterials, and metamaterials.

Previous studies on gamma-ray shielding can be broadly classified into three main categories. The first group focuses on experimental investigations, where attenuation coefficients and shielding parameters are measured for specific materials and configurations [4-8]. The second group involves theoretical and database-driven approaches, relying on tabulated photon interaction data and cross-sectional calculations, with foundational contributions. [9-29]. The third group includes simulation-based studies, often employing Monte Carlo techniques to model radiation transport and optimize shielding configurations [30-33]. While these approaches have significantly advanced the field, they are typically limited to material-specific analyses or case-dependent evaluations, rather than providing a unified comparative perspective.

Despite the availability of extensive photon interaction data, existing tables and datasets remain incomplete in practical terms, covering only a subset of elements and a limited range of compounds and mixtures [9,10, 25, 34]. Printed or tabulated data cannot fully accommodate the continuous variation of photon energy and often require interpolation, particularly near absorption edges, where discontinuities complicate accurate interpretation [35]. More importantly, most studies rely on absolute attenuation coefficients or isolated material comparisons, offering limited insight into the relative dominance of photon interaction mechanisms across different materials and energy ranges.

From an application perspective, this creates a practical challenge. Engineers and researchers must often select shielding materials for environments with varying radiation spectra, yet the available data does not provide an intuitive and comparative framework to identify which materials are most effective within specific energy regimes. This limitation becomes more pronounced in the design of multilayer or composite shielding systems, where different materials are expected to address different interaction mechanisms.

To address data accessibility and consistency, the XCOM web tool [36-39] provides a widely accepted platform for generating total and partial photon attenuation coefficients—including photoelectric absorption, coherent and incoherent scattering, and pair production—for elements (Z = 1–92) and selected compounds over a broad energy range from 1 keV to 100 GeV. For compounds, atomic weight fractions are derived from chemical composition, while for mixtures, user-defined weight fractions are applied. This database has become a standard reference in photon interaction studies due to its reliability and completeness.

In this context, the present study does not aim to reproduce existing cross-sectional data, but to systematically compile, normalize, and comparatively analyze photon interaction behaviors across a representative set of widely used materials spanning low-Z to high-Z regimes. The selected materials (B, Al, Si, Cu, W, Pb, water, and air) are not arbitrary; they reflect commonly used shielding materials, enabling physically meaningful comparisons across practical applications.

The effectiveness of gamma-ray shielding is governed by atomic number (Z), atomic weight (A), density (ρ), and photon energy (Eγ) [40]. High-Z, high-density materials such as lead (Pb, Z = 82, 11.35 g/cm³) and tungsten (W, Z = 74, 19.3 g/cm³) exhibit strong attenuation due to enhanced photoelectric absorption and pair production [45-48]. Medium- and low-Z materials, including aluminum (Al, Z = 13, 2.70 g/cm³) [41, 42] and silicon (Si, Z = 14, 2.33 g/cm³) [43, 44], provide structural advantages and contribute to the

moderation of secondary radiation. In addition, hydrogen-rich and neutron-interacting materials such as boron (B, Z = 5, 2.37 g/cm³) [45, 46], water [47, 48], and air [49, 50] play an important role in mixed radiation environments, particularly in nuclear facilities and space applications.

By introducing dominance-based visualization, this study reveals that the variation of photon interaction mechanisms is not random but follows systematic and predictable trends governed by atomic number and photon energy. These trends are often difficult to recognize when materials are examined individually.

The main contribution of this work is therefore the development of a comparative and visually interpretable framework that highlights the relative dominance of photoelectric absorption, Compton scattering, and pair production over the energy range of 1 keV to 20 MeV. This energy range is not arbitrarily selected; rather, it is deliberately chosen to represent a broad spectrum spanning from medical applications to high-energy nuclear physics, including energies accessible in typical laboratory-scale experimental setups. This approach facilitates a clearer understanding of energy-dependent behavior and supports the preliminary evaluation and selection of materials for gamma-ray shielding applications.

2. MATERIALS AND METHODS

2.1 Selection of Shielding Materials

The materials chosen for the gamma-ray attenuation analysis were boron (B), aluminum (Al), silicon (Si), copper (Cu), tungsten (W), lead (Pb), water, and air. These materials represent a range of atomic numbers (Z), densities, and physical states, allowing for a comprehensive evaluation of their attenuation capabilities. The selected materials were intentionally chosen to represent practical and widely used shielding materials across different application domains (nuclear, medical, aerospace, and industrial). Thus, this selection is not arbitrary but designed to span a broad range of atomic numbers and densities, allowing the identification of systematic trends in photon interaction dominance.

2.2 Attenuation Mechanisms and Cross-Sections

This study focuses on the following primary gamma-ray interaction mechanisms: incoherent (Compton) scattering, coherent (Rayleigh) scattering, photoelectric absorption, and pair production. The respective cross sections (μ) for each process were analyzed for all selected materials. A coherent (Rayleigh) scattering cross-section occurs when gamma rays are scattered elastically by bound electrons in a medium. However, incoherent (Compton) scattering cross-sections occur where inelastic scattering occurs due to interactions with free or loosely bound electrons. On the absorption side, the photoelectric absorption cross section plays an important role in the complete absorption of gamma-ray photons, leading to electron emission. In comparison, the pair production cross section has a threshold energy of 1.022 MeV in both the nuclear and electron fields. The absorption part is somewhat questionable for pair production, because only energy $E_\gamma - 1.022\ MeV$ is transferred to the electron-positron pair. The remaining energy, 1.022 MeV, was obtained from two annihilation photons. Therefore, the medium does not deposit energy from these two annihilation photons if they escape. The energy provided by photons to electrons and positrons is usually considered to be absorbed in the medium during interaction. Charged particles, such as electrons in solid materials, such as tissues, play a crucial role in this assumption. However, Compton-scattered photons, X-rays, and annihilation photons can escape from the medium. All these factors affect the fraction of heat generated in shielding materials and the gamma radiation dose to humans because of gamma-ray absorption. The gamma-ray absorption coefficient helps calculate the deposited energy.

The total attenuation cross section, which is the sum of all interaction cross sections, considers both scattering and absorption. The total triplet production and photonuclear reaction cross-sections allocate a minor ratio; therefore, the XCOM database disregards them in their results. However, $\mu_{triplet\ production} + \mu_{photo\ nuclear}$ could be added for more complex analyses in the future, depending on experimental needs. The relevant equation for this sum is as follows:

$$\mu_{total} = \mu_{incoherent\ Compton} + \mu_{coherent\ Rayleigh} + \mu_{photoelectric} + \mu_{pair\ production} \quad (1)$$

The relative dominance indicates a comparative study of the prevailing attenuation mechanism for each material across various energy levels. To show the relative contributions for each element and mixture, the total cross-section for each interaction was calculated at each gamma-ray energy and then converted to a dominance percentage using the stacked bar approach instead of heat map visualization. The same method can be used if a specific combination of compounds or mixtures is required. Thus, either the scattering or absorption rate can be estimated experimentally in a particular case.

The cross-sections for the photoelectric effect, Compton scattering, and pair production can be estimated using semi-empirical relationships based on atomic number Z, photon energy E_γ, and density ρ, as described by Tsoulfanidis and Landsberger [41]. The attenuation coefficients are expressed as follows:

$$\tau(m^{-1}) = a\left(\frac{N_A\rho}{A}\right)\left(\frac{Z^n}{E_\gamma^m}\right)[1 - O(Z)] \quad (2)$$

$$\sigma(m^{-1}) = \rho\frac{N_A}{A}Zf(E_\gamma) \sim \rho\frac{N_A}{2}f(E_\gamma) \quad (3)$$

$$\mathrm{K}(m^{-1}) = \rho\frac{N_A}{A}Z^2f(E_\gamma, Z) \quad (4)$$

where:

- τ, σ, K are the linear attenuation coefficients (in m^{-1}) for photoelectric absorption, Compton scattering, and pair production, respectively,
- a is a constant independent of Z and E_γ,
- N_A is Avogadro's number (6.022×10^{23} mol^{-1}),
- ρ is the material density (kg/m^3),
- A is the atomic mass (g/mol),
- f(E_γ), f(E_γ, Z) are energy-dependent functions (Compton and pair production),
- O (Z) is a small correction term,
- n and m are the empirically determined exponents.

To compare the materials, the following scaling relationships can be applied:

$$\tau_2(m^{-1}) = \tau_1\frac{\rho_2}{\rho_1}\left(\frac{Z_2}{Z_1}\right)^n \quad (5)$$

$$\sigma_2(m^{-1}) = \sigma_1\frac{\rho_2}{\rho_1}\left(\frac{A_1}{A_2}\right)\left(\frac{Z_2}{Z_1}\right) \quad (6)$$

$$\mathrm{K}_2(m^{-1}) = \mathrm{K}_1\frac{\rho_2}{\rho_1}\left(\frac{A_1}{A_2}\right)\left(\frac{Z_2}{Z_1}\right)^2 \quad (7)$$

Finally, the mass attenuation coefficient was obtained by dividing the linear coefficient by material density.

$$\mu\left(\frac{m^2}{kg}\right) = \frac{\mu(m^{-1})}{\rho(kg/m^3)} \quad (8)$$

These semi-empirical relations, drawn from Tsoulfanidis and Landsberger [41], provide a foundational understanding of the photon interaction behavior and scaling in different media.

2.3 Data Collection and Computational Analysis

Data for the interaction cross sections and attenuation coefficients were sourced from the NIST XCOM database. The attenuation coefficients of each material were plotted across different photon energy levels to visualize and compare their gamma-ray attenuation capabilities.

2.4 Comparison and Evaluation

A comparative analysis was conducted based on the following parameters: variation in each cross-section with photon energy, effectiveness of each material in attenuating gamma rays at different energies, and suitability of each material for gamma shielding applications. It is important to emphasize that the purpose of these plots is not to reproduce XCOM data itself, but to enable cross-material comparison and reveal systematic trends in interaction dominance across different energy regimes.

2.5 Graphical and Statistical Representation

The results are presented using graphs that illustrate the energy-dependent cross-sections for each material, alongside bar charts that compare the relative attenuation capabilities across all selected materials. Absolute cross-section values were obtained from the NIST XCOM database, and the relative contributions of each material were calculated by normalizing their cross-sections to the total at each photon energy. No interpolation was applied in this study; all analyses were performed using the discrete energy points directly obtained from the XCOM database. This approach preserves the intrinsic structure of the tabulated data and avoids potential inaccuracies associated with interpolation, particularly near absorption edges where discontinuities are physically meaningful. Since the dataset is deterministic and derived from evaluated theoretical calculations, statistical uncertainty analysis was not applicable. The analysis focuses on identifying relative trends and dominance behavior as a function of photon energy, rather than statistical variability. Data processing and visualization were performed in Excel, enabling systematic identification of dominant interaction mechanisms and trends across the energy spectrum. This methodology provides a clear and quantitative understanding of gamma-ray attenuation behavior, facilitating the selection of optimal shielding materials for various radiation protection applications.

3. RESULTS and DISCUSSIONS

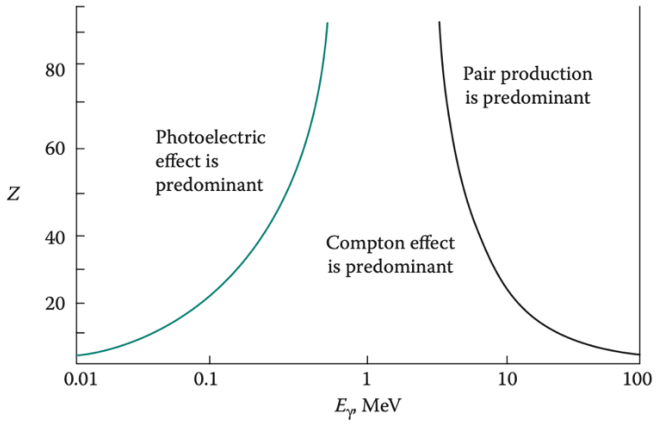

Figure 1. Relative Importance of Three Major Gamma Interactions [41]

Figure 1 shows the dominant interaction mechanisms for gamma-ray attenuation as a function of the photon energy (hv in MeV) and atomic number (Z) of the absorber. The key observations for the low-, medium-,

and high-energy regions are as follows: Low energy region below ~0.5 MeV, the photoelectric effect is the dominant interaction mechanism. This effect is highly dependent on Z ($\sigma \propto Z^4$–Z^5), meaning high-Z materials (like Pb, W, and Cu) are very effective at low energies. Regarding shielding, Lead (Pb) and Tungsten (W) are excellent gamma-ray shields in this range because of their high Z. For the intermediate energy region in the range of 0.5 to ~5 MeV, Compton scattering dominates, and attenuation becomes less dependent on Z. Here, material density becomes more critical than atomic number. For shielding insights, medium-Z materials such as Cu, Si, and Al can be effective; however, high-density materials (such as W and Pb) are still preferable. Finally, in the high-energy region, where the photon energies are greater than ~5 MeV, pair production is the main interaction process. This effect is strongly dependent on Z and favors high-Z materials. Very high-Z materials such as W and Pb are the best choices for shielding high-energy gamma rays.

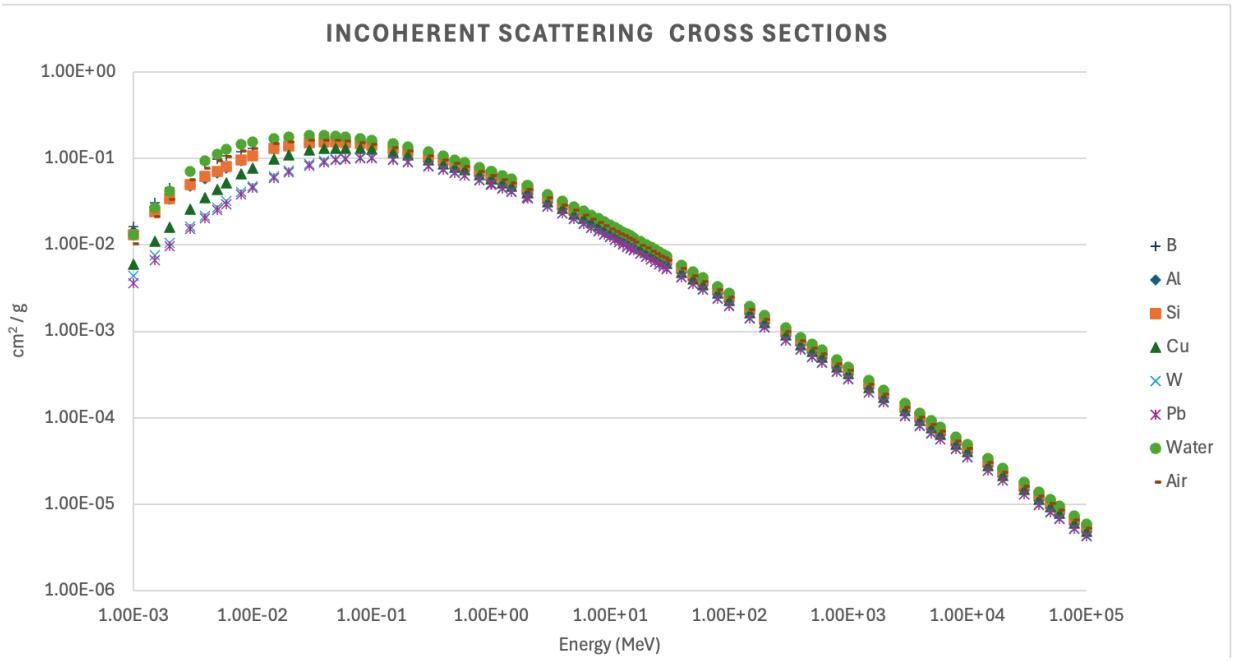

Figure 2. Incoherent Scattering Cross-Sections of Selected Elements and Materials (B, Al, Si, Cu, W, Pb, water, and air) as a Function of Gamma Ray Energy

Figure 2 presents the incoherent (Compton) scattering cross-sections in units of cm^2/g as a function of gamma ray energy (MeV) for various shielding materials, including B, Al, Si, Cu, W, Pb, water, and air. In terms of peak cross sections at low to intermediate energies (~0.01–1 MeV), the incoherent scattering cross section increases with energy at low energies, reaches a peak, and then gradually decreases at higher energies.

This behavior was expected because Compton scattering is the dominant interaction mechanism in the mid-energy range (~0.1–10 MeV). The data points for different materials closely overlap, meaning that when normalized per gram, the incoherent scattering behavior is similar across materials. This is because Compton scattering is dependent on electron density, which is relatively constant per unit mass for most materials. It's also clear in Eq. 3. High-Z materials such as Pb and W do not show a drastically higher cross-section per gram compared to low-Z materials such as Al and Si. In the high-energy region (>10 MeV), the incoherent scattering cross section steadily decreases as the energy increases. At very high energies (>100 MeV), pair production (instead of Compton scattering) becomes dominant, leading to a further drop in the Compton cross section. Regarding the comparison of shielding materials, the advantages of Lead (Pb) and tungsten (W) as shielding materials are due to their higher density, because the cross-section per gram is similar for all materials. Lead (Pb, 11.34 g/cm^3) and tungsten (W, 19.25 g/cm^3) provide more attenuation per unit volume than lighter materials, such as aluminium or water. Low-Z materials (boron, aluminium, silicon, air, and water) have a similar cross-section per gram but much lower densities, making them less effective as gamma-ray shields. However, materials, such as water and air, can contribute to radiation scattering and energy dissipation.

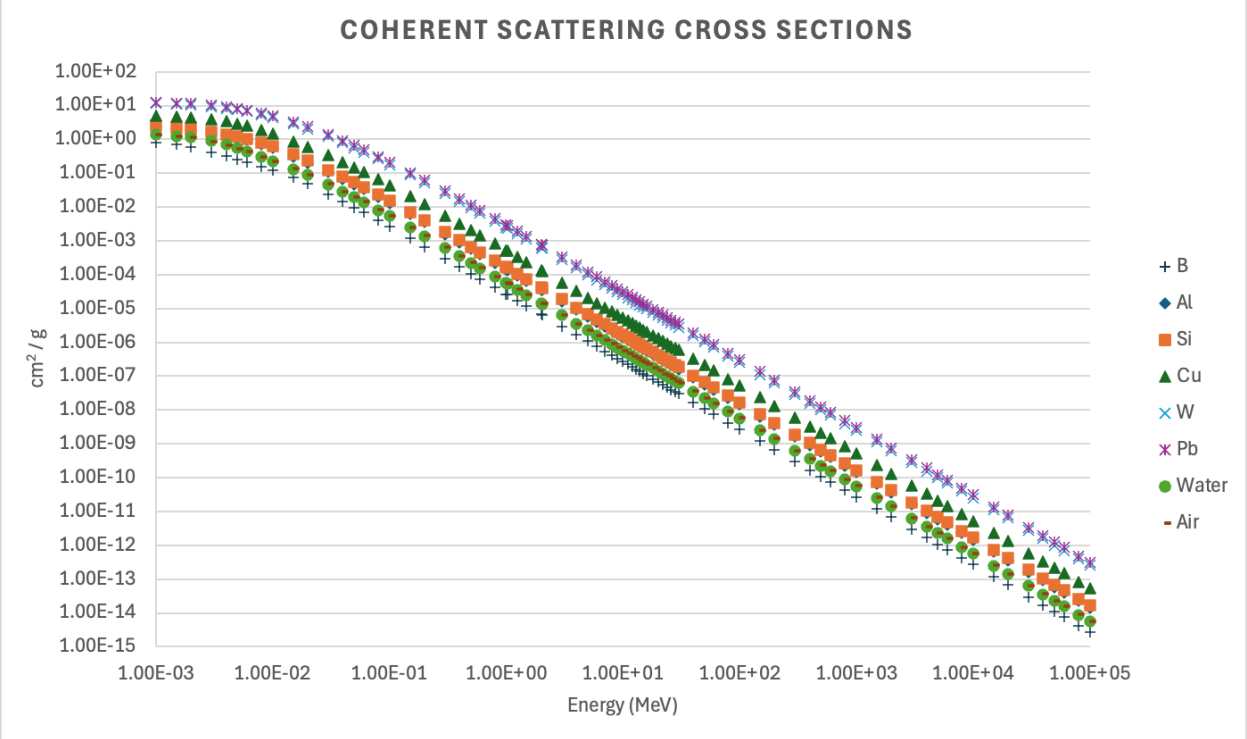

Figure 3. Coherent Scattering Cross-Sections of Selected Elements and Materials (B, Al, Si, Cu, W, Pb, water, and air) as a Function of Gamma Ray Energy

Figure 3 shows coherent (Rayleigh) scattering cross-sections as a function of gamma-ray energy, which contrasts with the previous plot of incoherent (Compton) scattering. The key difference is that coherent scattering is significant only at low energies and decreases rapidly as the energy increases, whereas incoherent scattering dominates in the mid-energy range (~0.1–10 MeV) and declines more gradually. Coherent scattering involves elastic photon interactions without energy loss, making it more relevant for low-energy photons, whereas incoherent scattering results in energy transfer and is the primary interaction for mid-energy gamma-rays. High-Z materials, such as Pb and W, show higher coherent scattering cross-sections but remain less relevant for shielding compared to incoherent scattering, which plays a greater role in attenuation at practical gamma-ray energies.

In Figure 4, the cross-sections are given in cm^2/g, which indicates the effective area for absorption per unit mass of the material. This unit is useful because it allows the comparison of different materials regardless of their density. The energy of the gamma rays is given in MeV, ranging from 1.00E-03 MeV to 1.00E+05 MeV. This is a broad range, covering low-to high-energy gamma-rays. The materials listed (B, Al, Si, Cu, W, Pb, water, and dry air) have different atomic numbers and densities, which affect their photoelectric absorption cross sections. Generally, materials with higher atomic numbers (such as lead) have higher cross sections at lower energies owing to the stronger interaction between gamma rays and atomic electrons. Typically, the photoelectric absorption cross section decreases as the energy of the gamma rays increases. This is because higher-energy photons are less likely to be absorbed by electrons in the material. The cross-section can also show sharp decreases at certain energy levels, known as absorption edges, which correspond to the binding energies of the inner electrons in the atoms. Figure 4 depicts how the cross sections vary across different energy levels, typically plotted on a logarithmic scale to capture a wide range of values. In contrast, lighter materials, such as water and dry air, show much lower cross sections across the entire energy range, making them less effective at attenuating gamma rays compared to heavier elements. This plot is crucial for applications in radiation shielding, medical imaging, and astrophysics because it helps in selecting appropriate materials based on their absorption properties at specific gamma ray energies.

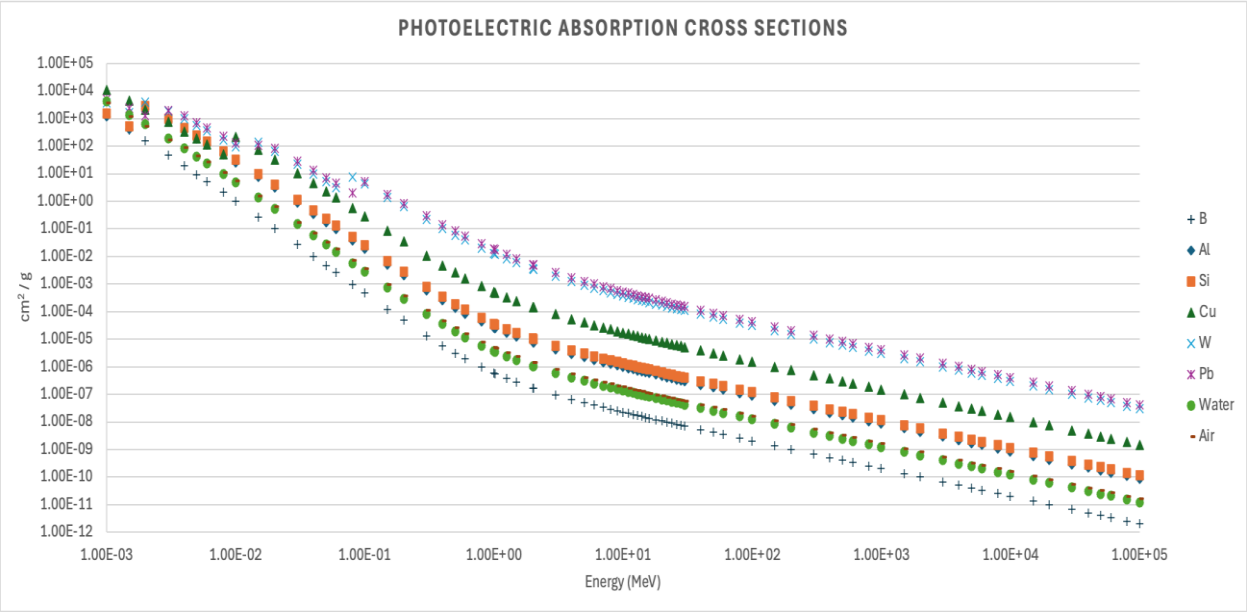

Figure 4. Photoelectric Absorption Cross-Sections of Selected Elements and Materials (B, Al, Si, Cu, W, Pb, water, and air) as a Function of Gamma Ray Energy

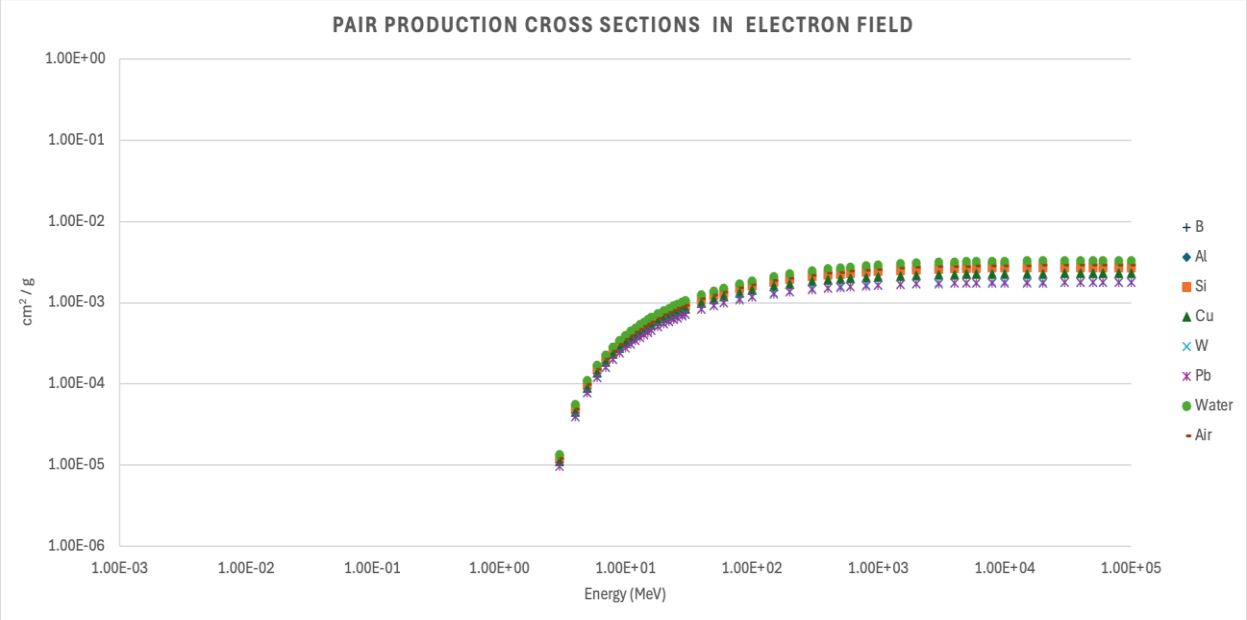

Figure 5. Pair Production Cross-Sections in the Electron Field of Selected Elements and Materials (B, Al, Si, Cu, W, Pb, water, and air) as a Function of Gamma Ray Energy

Figure 5 illustrates the pair production cross sections in the electron field for different materials plotted against the gamma-ray energy in MeV. Pair production becomes significant at higher gamma-ray energies, typically above 1.022 MeV, which is the threshold energy required to create an electron-positron pair. As the energy increased beyond this threshold, the cross-section for pair production generally increased, reflecting a higher probability of this interaction. Electron density per gram refers to the number of electrons per unit mass of the material. This is calculated as follows: $n_e = \frac{NZ}{\rho} = \frac{Z}{A} \times N_A$. The Z/A ratio determines the number of electrons per unit of mass. The decreasing Z/A ratios of the selected materials were calculated as follows: 0.799 for water, 0.510 for dry air, 0.5 for Si, 0.482 for Al, 0.463 for B, 0.456 for Cu, 0.403 for W, and 0.396 for Pb in mole/g unit. The same order of magnitude is valid for the electron densities per gram (n_e). Light elements have a higher Z/A ratio, meaning that they contain more electrons per gram than

heavier elements do. Heavier elements (e.g., Pb and W) have lower Z/A values because their atomic masses grow faster than their atomic numbers. Pair production occurs because of interactions with electrons, as shown in Figure 5. If a material has more electrons per gram, it offers more interaction sites per unit mass, leading to a higher mass-attenuation coefficient. Water (H_2O) and air (mostly N_2 and O_2) have a high electron density per gram, explaining why they have larger cross-sections per unit mass than Pb or W. This aligns with what we see in the plot: water and air show the highest pair of production cross-sections per gram, despite being low-Z materials.

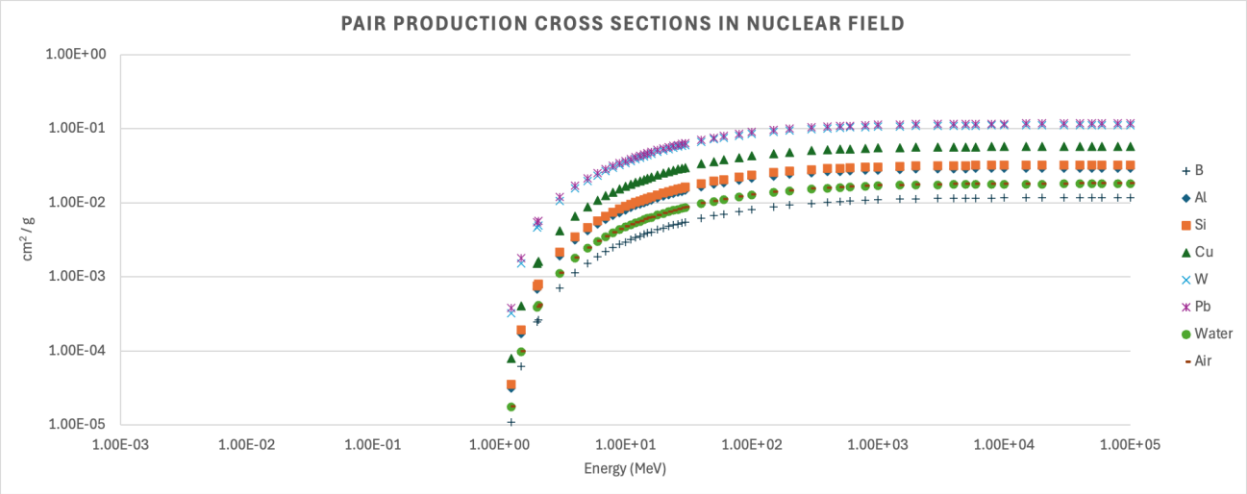

Figure 6. Pair Production Cross-Sections in the Nuclear Field of Selected Elements and Materials (B, Al, Si, Cu, W, Pb, water, and air) as a Function of Gamma Ray Energy.

The plot of the pair production cross sections in the nuclear field in Figure 6 shows the probability of gamma rays converting into electron-positron pairs when interacting with the electric field of a nucleus, typically for energies above 1.022 MeV. This process is more significant in materials with high atomic numbers, such as tungsten (W) and lead (Pb), owing to their stronger nuclear electric fields, resulting in higher cross-sections compared to pair production in the electron field. In contrast, pair production in the electron field, where gamma rays interact with the electric field of electrons, generally has lower cross sections because the electron field is weaker. Both processes increase with the gamma-ray energy, but the nuclear field process dominates at higher energies. Understanding these differences is essential for applications in radiation shielding and medical imaging, where material selection and interaction mechanisms are critical for effective gamma ray attenuation and detection.

The values for the total attenuation cross-sections with and without coherent scattering in Figures 7 and 8 appear almost the same across the provided energy range. This suggests that coherent scattering, photoelectric absorption, and pair production have either minimal or no contribution owing to the threshold energy of the total attenuation. This is because they are aligned in close proximity to the low-energy range of up to 10^{-1} MeV. In contrast, incoherent scattering was more distinct in the same low-energy interval. In the intermediate energy range (10^{-1}-10 MeV), coherent scattering and photoelectric effects have more distinctive values. The pair production in the nuclear and electron fields begins to change the total attenuation after 1.022 MeV. The first has a more dominant addition than the second to the total cross-section.

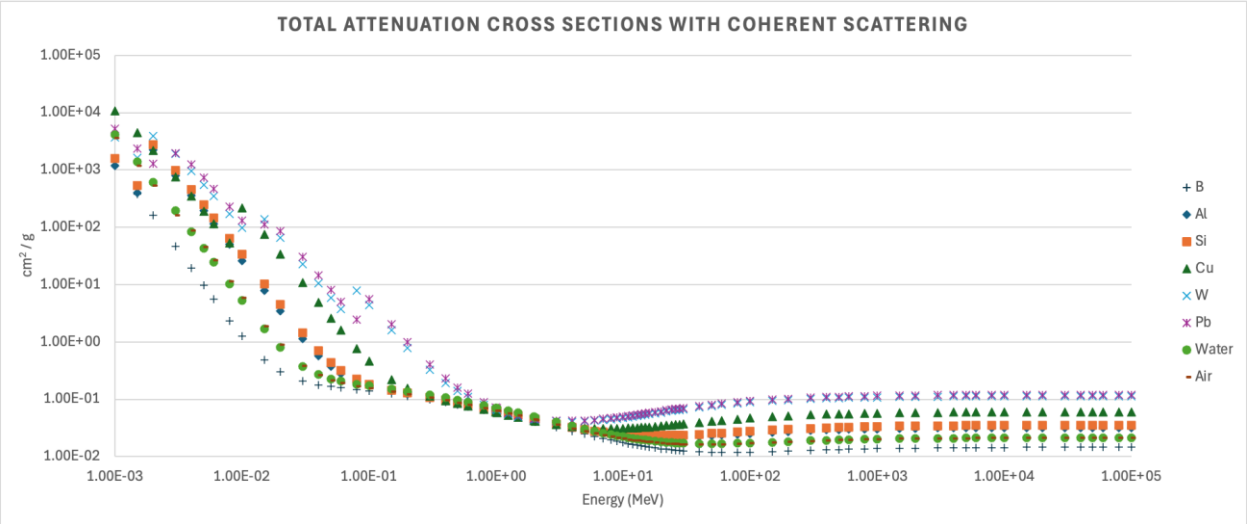

Figure 7. Total Attenuation Cross-Sections with Coherent Scattering of Selected Elements and Materials (B, Al, Si, Cu, W, Pb, water, and air) as a Function of Gamma-Ray Energy.

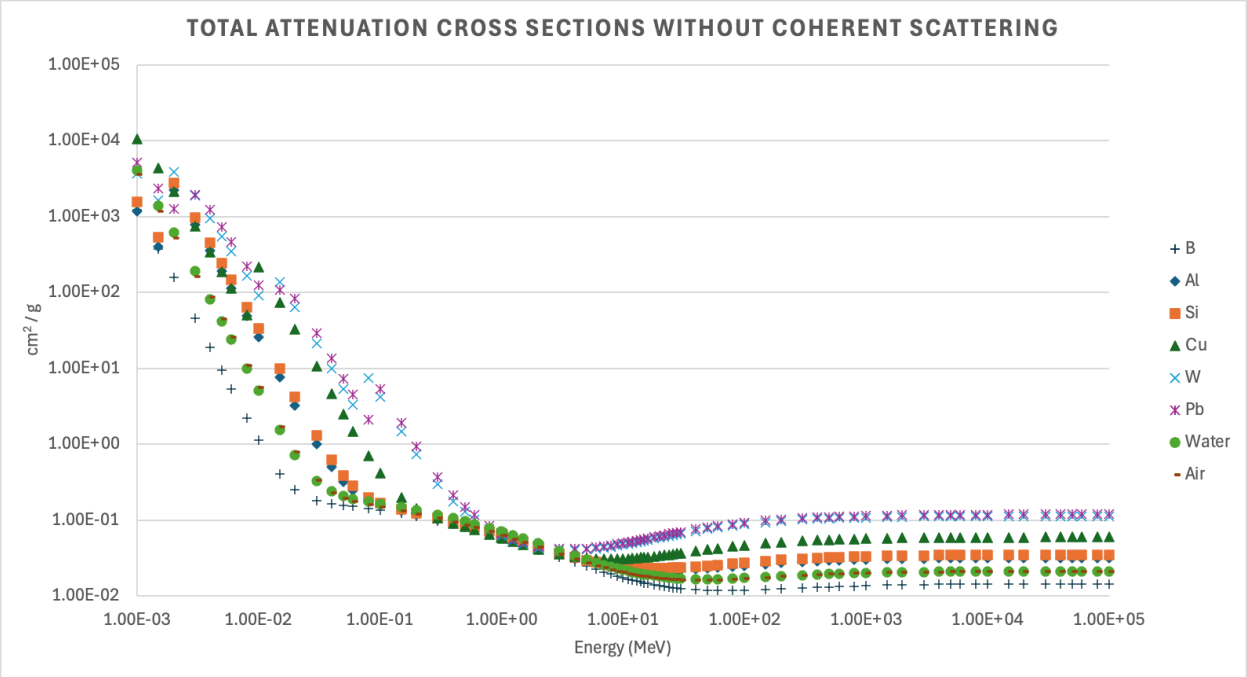

Figure 8. Total Attenuation Cross Sections Without Coherent Scattering of Selected Elements and Materials (B, Al, Si, Cu, W, Pb, water, and air) as a Function of Gamma-Ray Energy.

The near-identical values for the total attenuation cross-sections with and without coherent scattering for a chosen material across the provided energy range indicate that coherent scattering after 10 MeV was almost negligible. The order of magnitude of the total cross-sections was as follows: Pb > W > Cu > Si > Al > water > air > B.

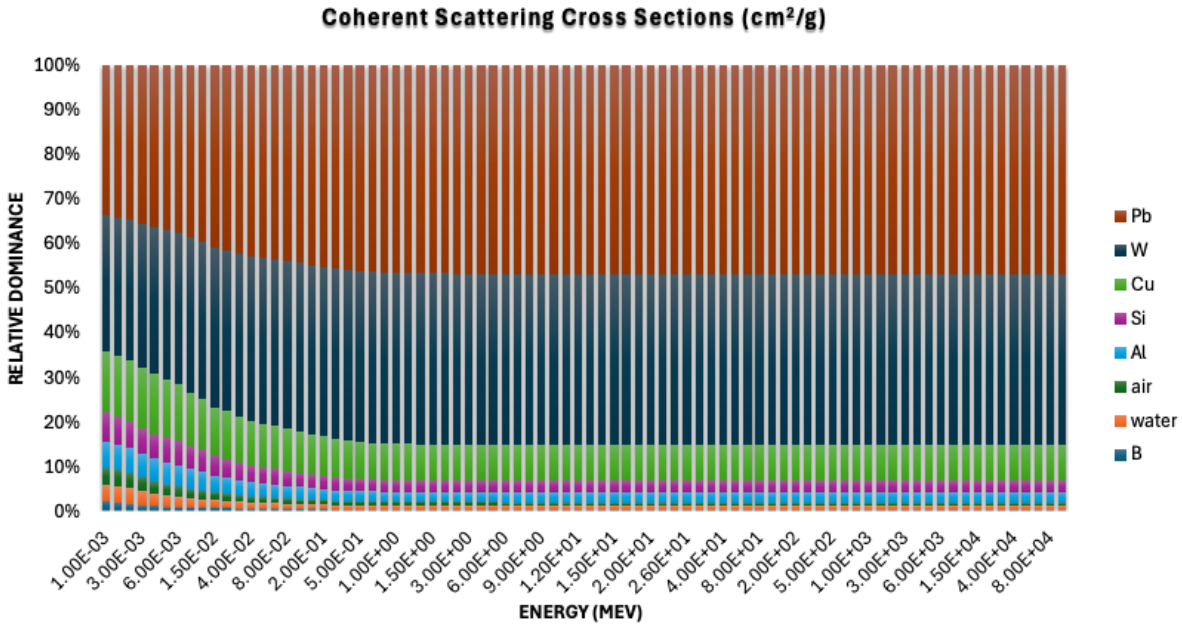

Figure 9. Relative Dominance of Coherent Scattering Cross Sections of Selected Elements and Materials (B, Al, Si, Cu, W, Pb, water, and air) as a Function of Gamma-Ray Energy

The data in Figure 9 show the relative contributions of various materials (B, water, air, Al, Si, Cu, W, and Pb) to the total cross-section at different photon energies, normalised so that the total sum is 1.00 at each energy. At lower energies (below 0.1 MeV), high-Z materials, such as tungsten (W) and lead (Pb), dominate because of their strong coherent scattering, contributing significantly (e.g., W: ~0.306, Pb: ~0.335 at 1.00E-03 MeV). Intermediate-Z materials such as copper (Cu), silicon (Si), and aluminum (Al) have moderate contributions at these energies, whereas low-Z materials such as boron (B), water, and air contribute minimally. As the photon energy increased, the relative contribution of the high-Z materials decreased and the differences between the materials became less pronounced. At higher energies (above 1 MeV), coherent scattering becomes negligible, and the contributions of all the materials stabilize at low fractions. These data highlight the importance of the material composition and photon energy in determining the relative dominance of different interaction mechanisms, which is crucial for applications in radiation shielding, medical imaging, and nuclear physics.

In Figure 10, at very low photon energies (1-10 keV), incoherent scattering values are more variable, with boron (B), water, and air showing higher contributions than heavier elements such as lead (Pb) and tungsten (W). As the photon energy increased, the relative contributions stabilized, with all materials converging to nearly the same value (~0.123–0.148) above ~100 keV. This suggests that, at high energies, incoherent scattering dominates uniformly across materials, regardless of the atomic number. At low energies, photoelectric absorption is dominant and incoherent scattering varies significantly between the elements. As the energy increases, Compton scattering becomes the primary interaction mechanism, leading to convergence of the values. In conclusion, at low gamma ray energies, incoherent scattering is more material-dependent, with lighter elements exhibiting higher fractions. As the energy increases beyond ~100 keV, incoherent scattering becomes nearly independent of the material composition, showing a stable contribution across all substances. For practical applications, such as shielding, the Compton scattering effects become uniform at high gamma-ray energies.

The dataset in Figure 11 presents the relative dominance of the photoelectric absorption cross section for various materials as a function of photon energy (gamma energy). The materials included boron (B), water, air, aluminum (Al), silicon (Si), copper (Cu), tungsten (W), and lead (Pb), with the sum of all contributions normalized to 1.00. At low photon energies (1.00E-03 to 1.50E-03 MeV), the photoelectric effect is most dominant in copper (Cu), tungsten (W), and lead (Pb), with Cu showing the highest contribution around

0.36 at 1.50E-03 MeV. As the energy increased to 2.00E-03 MeV, a shift occurred, and tungsten started to gain more influence, whereas lighter elements such as aluminum and silicon contributed more significantly.

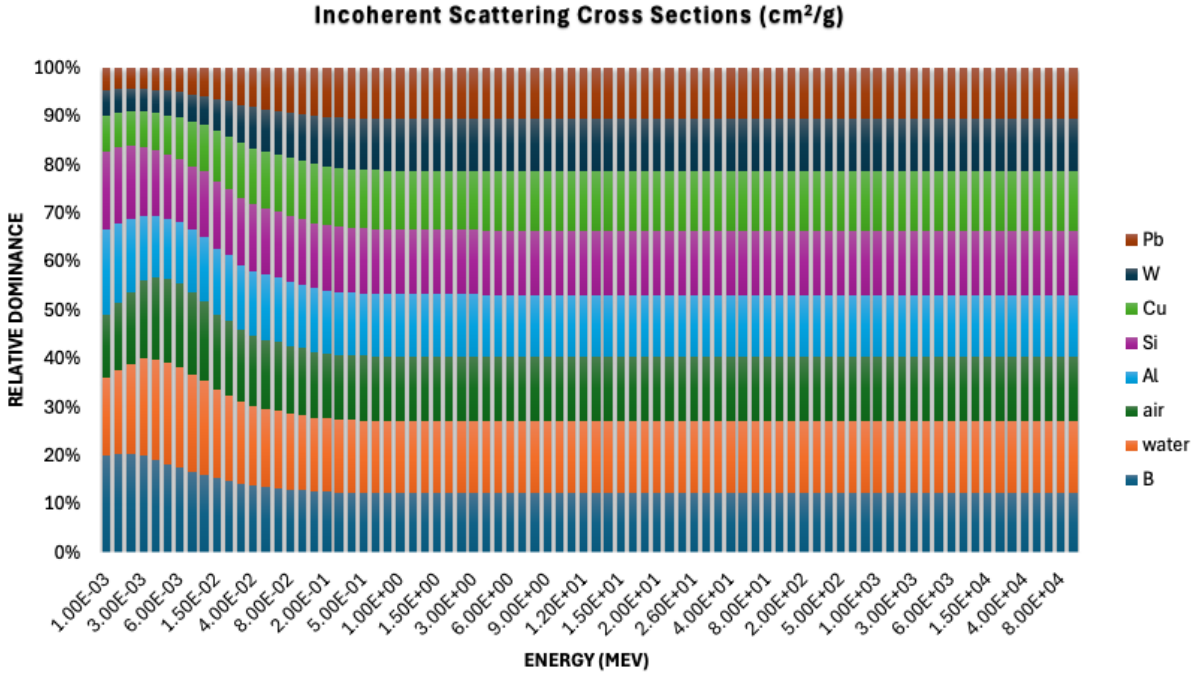

Figure 10. Relative Dominance of Incoherent Scattering Cross Sections of Selected Elements and Materials (B, Al, Si, Cu, W, Pb, water, and air) as a Function of Gamma-Ray Energy

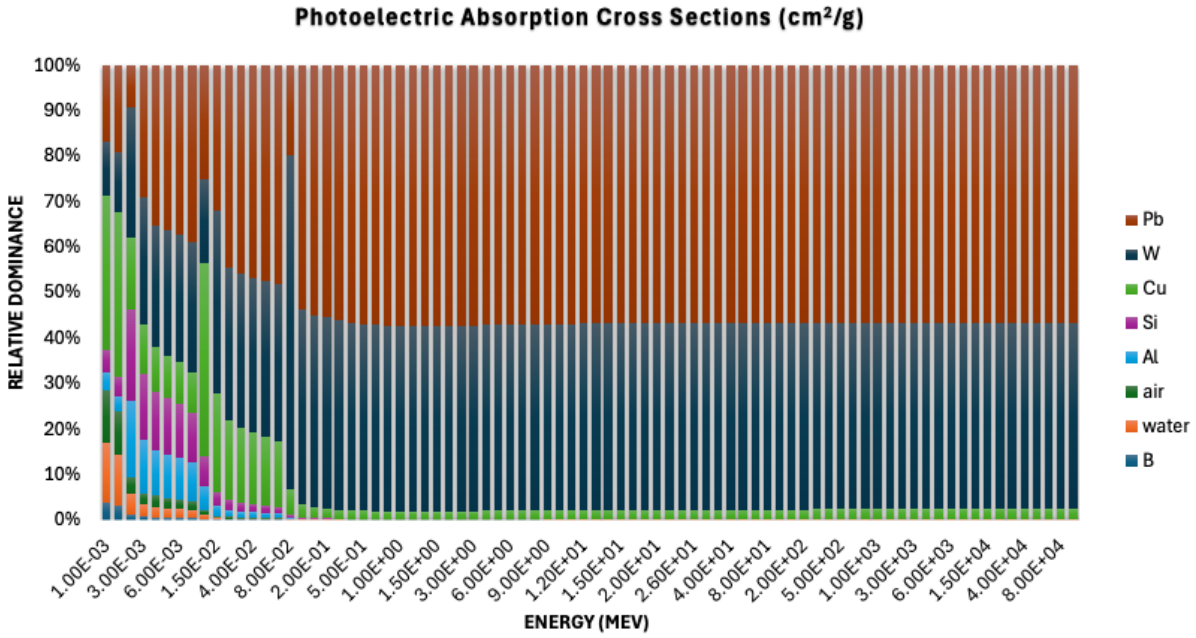

Figure 11. Relative Dominance of Photoelectric Absorption Cross Sections of Selected Elements and Materials (B, Al, Si, Cu, W, Pb, water, and air) as a Function of Gamma-Ray Energy

Between 3.00E-03 MeV and 1.00E-02 MeV, the dominance of heavy elements (W and Pb) remained, whereas boron and water showed minimal contributions. At approximately 8.00E-03 MeV, copper momentarily dominates; however, beyond this energy, tungsten (W) and lead (Pb) become the primary contributors, indicating their higher atomic number dependence on photoelectric absorption.

At intermediate energies (1.50E-02 to 1.00E-01 MeV), lead (Pb) starts to increase, reaching approximately 0.54 by 1.00E-01 MeV. Simultaneously, tungsten (W) also remained significant, while the influence of lighter materials diminished.

For higher photon energies (0.15 MeV and above), tungsten (W) and lead (Pb) overwhelmingly dominate, with Pb contributing around 0.57 and W around 0.41 at 1.00 MeV. Other materials, such as aluminum, silicon, and water, contribute negligibly to these energies.

Overall, the dataset highlights that at low gamma energies, mid-Z elements, such as Cu, play a key role, whereas at higher energies, high-Z elements, such as W and Pb, overwhelmingly dominate the photoelectric absorption because of their greater probability of interaction with photons. This trend aligns with theoretical expectations, as the photoelectric cross-section scales approximately from Z^3 to Z^4, making high-Z materials significantly more effective at absorbing lower-energy gamma photons.

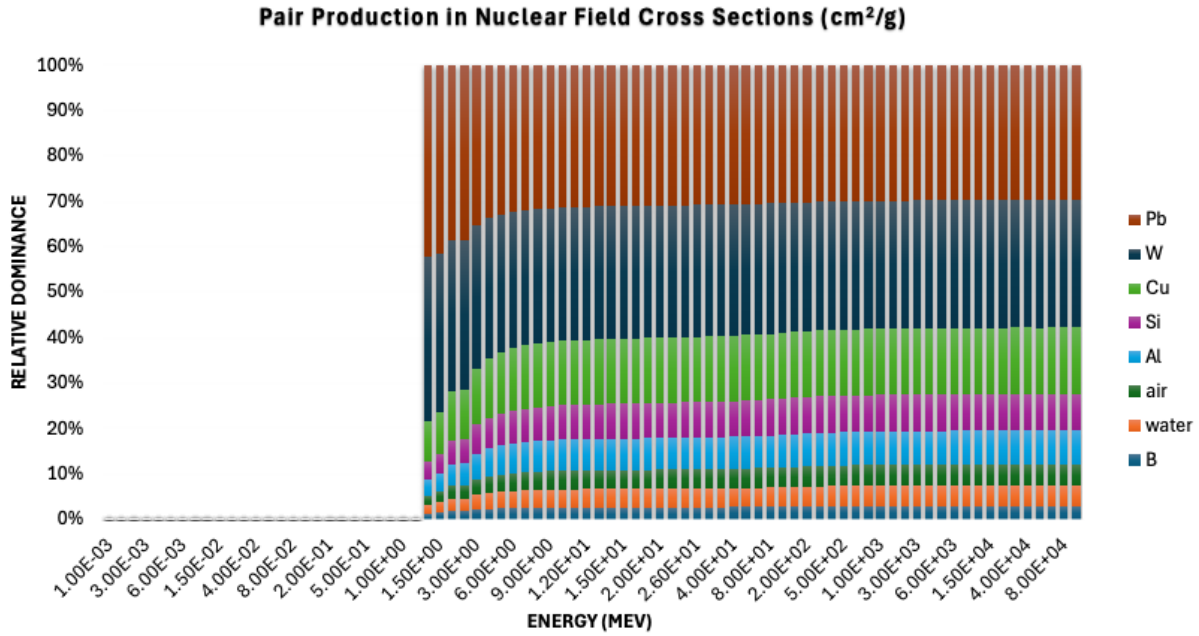

Figure 12. Relative Dominance of Pair Production in Nuclear Field Cross-Sections of Selected Elements and Materials (B, Al, Si, Cu, W, Pb, water, and air) as a Function of Gamma Ray Energy

The dataset in Figure 12 represents the normalized relative cross-section of pair production for various materials (Boron, Water, Air, Aluminum, Silicon, Copper, Tungsten, and Lead) across gamma-ray energies from 1.25 MeV to 1.00E+05 MeV. Pair production, which requires a minimum gamma ray energy of 1.022 MeV, becomes increasingly significant at higher energies. High-Z materials, such as lead (Pb) and tungsten (W), dominate pair production because of their strong nuclear electric fields. For example, at 1.25 MeV, Lead (Pb) has a normalized relative cross section of 0.423, which decreases slightly to 0.313 at 10 MeV. This decrease occurs because while pair production increases with energy, other interaction mechanisms (such as Compton scattering) also become more significant, reducing the relative dominance of pair production. Medium-Z materials such as copper (Cu) and aluminum (Al) show moderate contributions, whereas low-Z materials such as boron (B) and water exhibit minimal contributions, with values increasing only slightly (e.g., B from 0.012 at 1.25 MeV to 0.025 at 10 MeV). The total strength of the column remained constant at 1.00, confirming that the values were normalized and represented the relative contribution of each material to the total pair production cross-section. Overall, the data highlight that pair production is most significant for high-Z materials at intermediate energies (1–10 MeV), making materials such as Lead and Tungsten ideal for high-energy gamma ray shielding and detection applications.

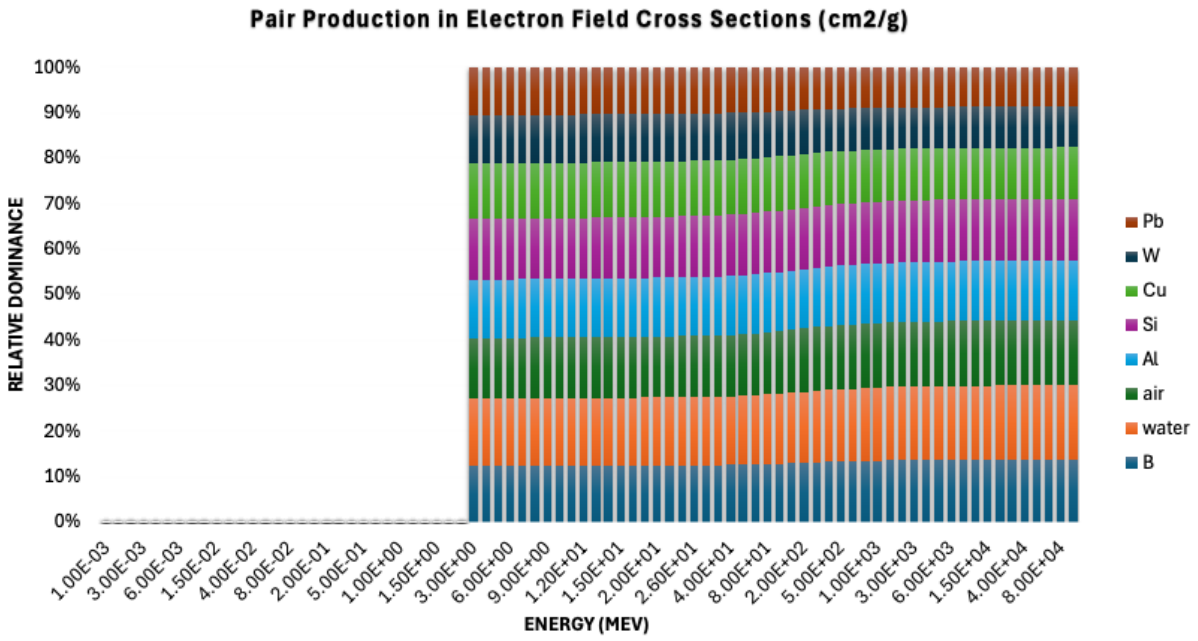

Figure 13. Relative Dominance of Pair Production in Electron Field Cross-Sections of Selected Elements and Materials (B, Al, Si, Cu, W, Pb, water, and air) as a Function of Gamma-Ray Energy.

Figure 13 shows the relative cross-section of pair production in an electron field for materials including boron, water, air, aluminum, silicon, copper, tungsten, and lead across gamma-ray energies. At 3.00E+00 MeV, the relative cross sections were boron (B) 0.123, water 0.148, air 0.133, aluminum (Al) 0.129, silicon (Si) 0.133, copper (Cu) 0.122, tungsten (W) 0.107, and lead (Pb) 0.105, with a total of 1.00. At 1.00E+01 MeV, the values are: B 0.124, Water 0.149, Air 0.133, Al 0.129, Si 0.133, Cu 0.122, W 0.106, and Pb 0.104, with a total of 1.00. At 1.00E+05 MeV, the values are: B 0.138, Water 0.162, Air 0.143, Al 0.132, Si 0.136, Cu 0.113, W 0.090, and Pb 0.087, with a total of 1.00. Low-Z materials, such as Boron, Water, and Air, exhibit an increase in the relative cross-section with energy (e.g., B from 0.123 to 0.138), whereas high-Z materials, such as tungsten and lead, exhibit a decrease (e.g., Pb from 0.105 to 0.087). Medium-Z materials, such as aluminum, silicon, and copper, remained relatively stable with slight variations (e.g., Cu from 0.122 to 0.113). This reflects the energy and material dependence of pair production in an electron field, with high-Z materials dominating at lower energies, and low-Z materials gaining significance at higher energies.

Pair production in a nuclear field and pair production in an electron field dataset exhibit distinct behaviors in terms of material and energy dependence. In the nuclear field, high-Z materials such as lead (Pb) and tungsten (W) dominate, with relative cross sections increasing with energy (e.g., Pb from 0.423 at 1.25 MeV to 0.467 at 10 MeV), whereas low-Z materials such as boron (B) and water have very low contributions (e.g., B from 0.012 to 0.025). In contrast, in the electron field, high-Z materials still dominate but show a decrease in the relative cross-section with energy (e.g., Pb from 0.105 at 3.00E+00 MeV to 0.087 at 1.00E+05 MeV), whereas low-Z materials, such as B and water, exhibit a significant increase (e.g., B from 0.123 to 0.138). Medium-Z materials, such as copper (Cu) and aluminum (Al), remain relatively stable in both fields, with slight variations (e.g., Cu from 0.122 to 0.113 in the electron field). These differences highlight the fact that high-Z materials are more effective for nuclear field-pair production at lower energies, whereas low-Z materials are more important in the electron field at higher energies. Both datasets reflect the energy and material dependence of pair production, with the nuclear field favoring high-Z materials and the electron field shifting toward low-Z materials as energy increases.

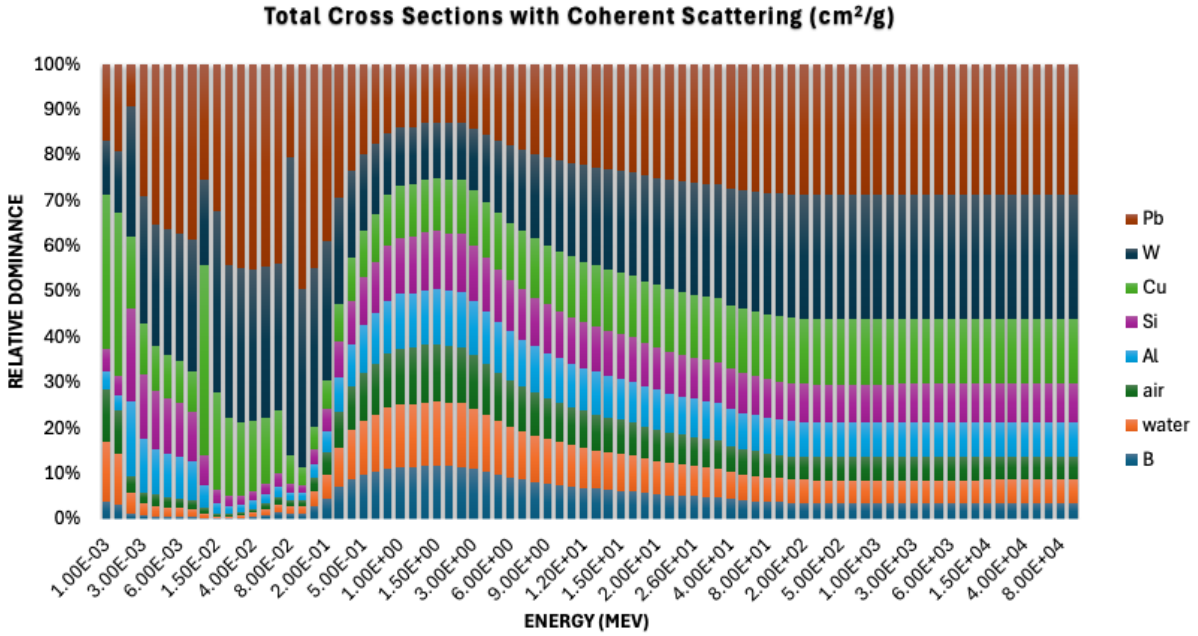

Figure 14. Relative Dominance of Total Cross-Sections with Coherent Scattering of Selected Elements and Materials (B, Al, Si, Cu, W, Pb, water, and air) as a Function of Gamma-Ray Energy

The dataset in Figure 14 for coherent scattering (Rayleigh scattering) provides insights into its relative contribution compared with the three major gamma interactions (photoelectric effect, Compton scattering, and pair production) across photon energies (1.00E-03 MeV to 1.00E+05 MeV) and materials. This is a structured interpretation aligned with Figure 1 from Evans' The Atomic Nucleus: At low energies (1.00E-03 MeV to 1.00E-02 MeV), lead (Pb) and tungsten (W) exhibit strong contributions (e.g., Pb: 0.167 at 1.00E-03 MeV, rising to 0.363 at 5.00E-03 MeV), reflecting their large atomic electric fields. Copper (Cu) peaks transiently at 0.419 at 1.00E-02 MeV, likely owing to resonance effects in the atomic shells. Compared to major interactions, coherent scattering complements the photoelectric effect, which typically dominates at low energies. High-Z materials were effective in both processes. At mid-energies (1.00E-01 MeV to 1.00E+01 MeV), high-Z materials (Pb, W) remained significant (Pb: 0.493 at 1.00E-01 MeV), but gradually declined as the energy increased. Low-Z materials (B, water, and air) show slight increases (B: 0.012 → 0.074), aligning with the rise in Compton scattering dominance in this range. Regarding material-specific behavior, medium-Z materials such as aluminum (Al) and silicon (Si) stabilize, indicating a reduced coherent scattering influence compared to Compton interactions. At High Energies (1.00E+01 MeV to 1.00E+05 MeV), a persistent high-Z contribution exists. Pb and W stabilized at moderate values (Pb: ~0.287, W: ~0.271 at 1.00E+05 MeV), unlike the steep decline in the photoelectric effect. Boron (B: 0.035) and water (0.051) remained minimal contributors, reflecting the dominance of pair production in the high-energy regimes.

Compared to Figure 1, the photoelectric effect dominates at low energies in high-Z materials, paralleling coherent scattering trends. Compton scattering peaks at mid-energies, thereby reducing the relative role of coherent scattering in mid-Z materials (e.g., Cu). Pair Production requires energies greater than 1.022 MeV, but coherent scattering in high-Z materials persists owing to atomic structure effects, unlike the photoelectric effect.

For material and energy dependence, high-Z materials (Pb, W) are critical for low-energy shielding (X-rays), owing to their strong coherent and photoelectric contributions. Medium-Z materials (Cu, Al) exhibit transient peaks (e.g., Cu at 1.00E-02 MeV), useful for specialized mid-energy applications. Low-Z materials (B, Water) have a minimal coherent scattering contribution, which aligns with their limited role in gamma ray interactions. Regarding practical implications, low-energy systems use Pb/W for shielding, leveraging coherent scattering and photoelectric absorption. Mid-energy applications balance Compton scattering and coherent effects, and Cu/Al may offer a niche utility. In high-energy physics, pair production

dominates, but coherent scattering in Pb/W remains non-negligible. In conclusion, although the three major interactions (photoelectric, Compton, and pair production) dominate the gamma-ray interactions, coherent scattering plays a supplementary role, particularly in high-Z materials at low-to mid-energies. The dataset underscores how the material choice and energy range dictate the relative importance of scattering mechanisms, with high-Z materials maintaining relevance even at ultrahigh energies owing to their atomic structures. This aligns with Evans' framework but highlights the unique persistence of coherent scattering compared to the photoelectric effect.

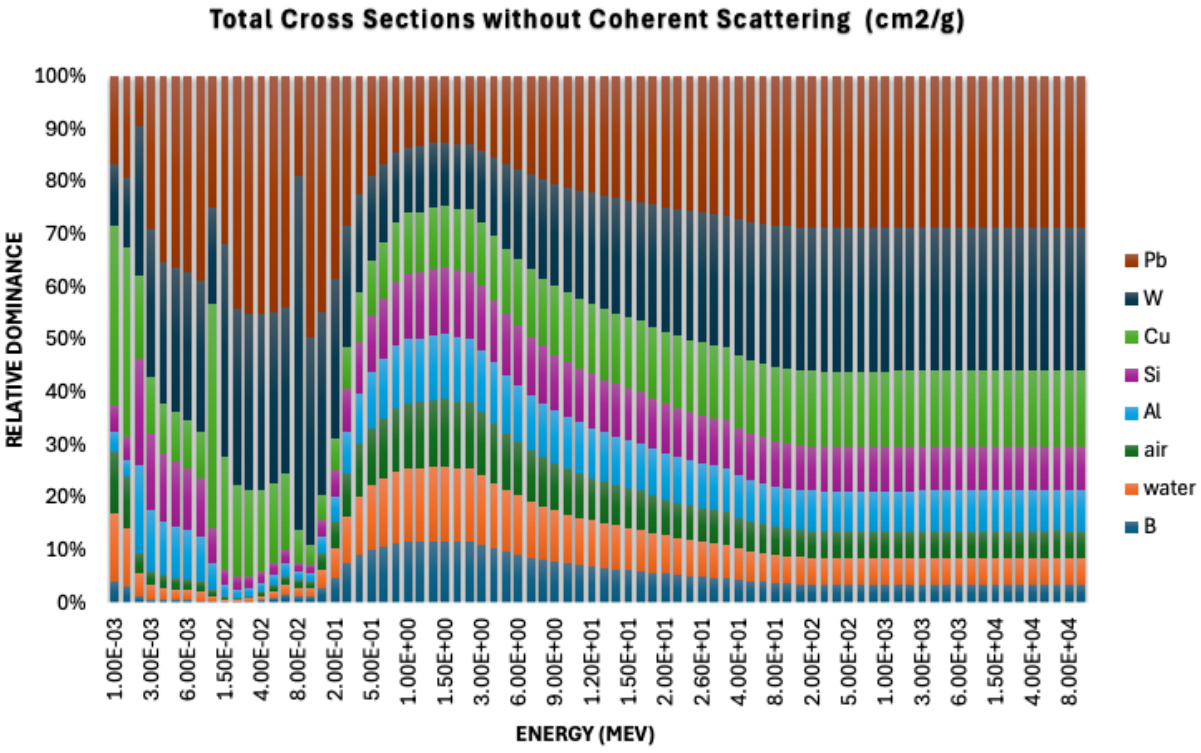

Figure 15. Relative Dominance of Total Cross Sections without Coherent Scattering of Selected Elements and Materials (B, Al, Si, Cu, W, Pb, water, and air) as a Function of Gamma-Ray Energy

The combination of Figures 8 and 15 provides a comprehensive understanding of the behavior of the total attenuation cross-sections (without coherent scattering) across a wide gamma-ray energy range. At low energies (below ~0.1 MeV), high-Z materials such as lead (Pb) and tungsten (W) dominate owing to strong photoelectric absorption, with cross-section values orders of magnitude higher than those of lighter materials such as boron, water, and air. As the energy increases (~0.1–2 MeV), Compton scattering becomes the dominant interaction, leading to a more balanced contribution across mid-Z materials, such as Al, Si, and Cu, although Pb and W still retain a significant portion. At high energies (>2 MeV), pair production begins to play a role, leading to a gradual increase in the cross-section values of high-Z materials, whereas lighter materials maintain relatively low attenuation. The relative dominance chart highlights the shift in contribution between different materials, showing that Pb and W remain the most effective for shielding across all energy ranges, whereas lighter materials become more relevant only at higher energies, where the cross-section values decrease overall. This analysis is crucial for applications in radiation shielding, medical imaging, and nuclear engineering, where material selection depends on the specific gamma-ray energy range of interest.

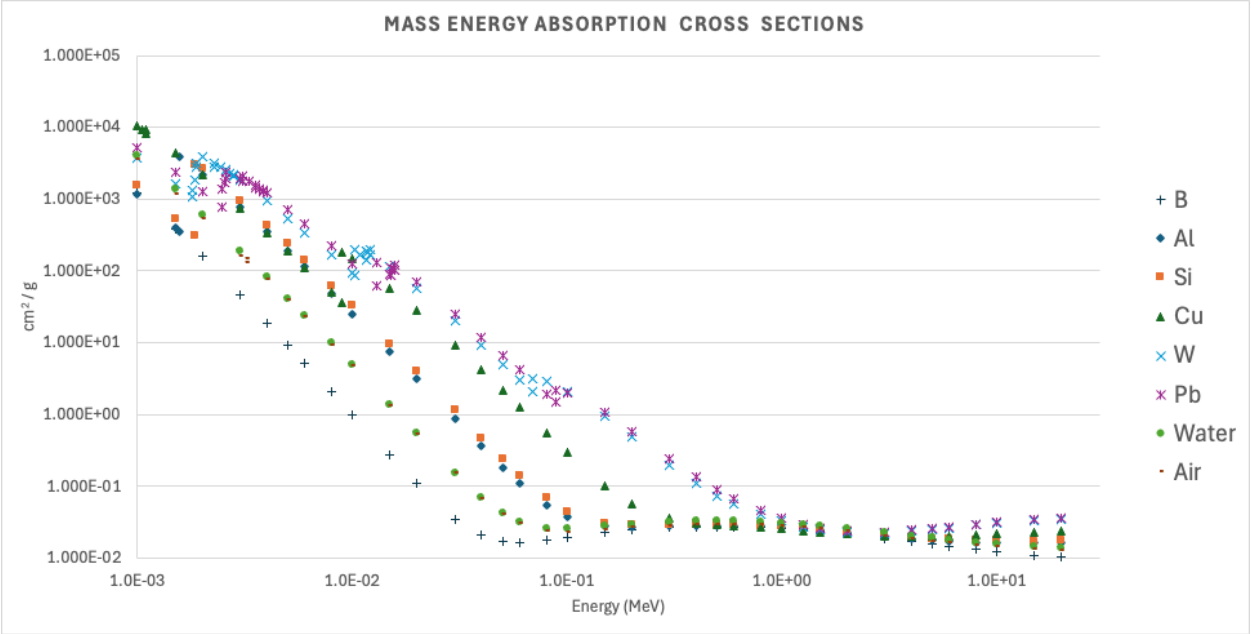

Figure 16. Mass Energy Absorption Cross Sections of Selected Elements and Materials (B, Al, Si, Cu, W, Pb, water, and air) as a Function of Gamma-Ray Energy

The dataset in Figure 16 with different energy ranges for each material reveals a fascinating correlation with the gamma ray interaction mechanisms shown in Figure 1. By analyzing these data, we can observe how the three dominant interaction processes— the photoelectric effect, Compton scattering, and pair production—manifest across different materials based on their atomic numbers (Z). For low-Z materials, such as boron, water, and air, the absorption coefficients decrease rapidly at low energies (1-10 keV) and then exhibit a more gradual decrease at higher energies, with the transition from photoelectric dominance to Compton scattering occurring at relatively low energies. In contrast, high-Z materials, such as W and Pb, exhibit extremely high absorption values at their K-edge energies (approximately 2-4 keV for tungsten and 3-4 keV for lead), after which there is a significant drop, followed by another transition to pair production dominance above approximately 5-10 MeV. The data for intermediate-Z materials such as aluminum, silicon, and copper show transitional behavior, with copper displaying pronounced absorption peaks at characteristic energy levels. These observations perfectly align with the first figure's representation of interaction mechanism dominance regions, where the photoelectric effect ($\propto Z^4$) dominates at low energies especially for high-Z materials, Compton scattering ($\propto \mathbf{Z}$) prevails in the mid-energy range with reduced Z-dependence, and pair production ($\propto Z^2$) becomes significant at higher energies for heavier elements—clearly demonstrating why lead and tungsten are preferred shielding materials for most radiation protection applications. However, keep in mind that they are toxic to humans.

If the fractions for each process are calculated and known in advance, each fraction is multiplied by the respective component of the mass attenuation coefficient $(\mu/\rho)_i$ for each interaction type i, and summing these products yields the mass energy absorption cross sections (μ_{en}/ρ). Again, the necessity of a multilayer approach that combines the right materials for the right radiation for specific energies is crucial for shielding.

4. APPLICATION INSIGHT: CASE FOR MULTI-LAYER SHIELDING IN SPACE MISSIONS

Space missions face a complex radiation environment comprising high-energy photons, protons, and secondary neutrons, which requires efficient lightweight shielding solutions. Multilayer shielding is a proven strategy that leverages the complementary properties of different materials to attenuate various radiation types while optimizing the mass and structural constraints.

A representative configuration may include the following.

• Outer layer – High-Z materials (e.g., tungsten and lead) to attenuate high-energy gamma photons via photoelectric and pair production interactions.

• Middle layer: Medium-Z materials (e.g., aluminum and copper) to scatter and moderate photon energy through Compton scattering.

• Inner layer: Hydrogen-rich materials (e.g., polyethylene, water, or borated polymers) to moderate and capture secondary neutrons.

This multilayered concept has been validated through several recent simulations and design studies. Sazali (2019) [51] showed that optimized three-layer shields (e.g., tungsten–polyethylene–aluminum) significantly reduced the radiation dose to spacecraft electronics in a geostationary orbit. Daneshvar et al. (2021) [52], using a combination of GEANT4 simulations and experimental setups, demonstrated that strategic layering of tungsten, aluminum, and polyethylene leads to notable dose reduction while maintaining acceptable weight. More recently, Guan et al. (2025) [53] explored the optimal thickness configurations for multilayer shielding of highly radioactive sources, emphasizing environmental safety and long-term storage.

Their study highlighted how optimized stacking of materials, such as lead and borated polyethylene, provides both gamma and neutron attenuation, with each layer contributing effectively to the total shielding.

A key insight from these studies is that the order of the layers in a multilayer shield does not affect the total transmission if the material thickness and properties are preserved. The exponential attenuation law governed the cumulative shielding effect.

$$I(t) = I_0 e^{-(\mu_1 t_1 + \mu_2 t_2 + \cdots)} \tag{9}$$

This expression shows that attenuation is commutative and multiplicative in the exponent: each layer contributes independently with $\boldsymbol{\mu}$ linear attenuation coefficient and thickness (t), and their combined effect depends only on the total attenuation path—not on the sequence of materials. This allows for practical flexibility in shield design based on the structural, thermal, or engineering requirements.

Dominance charts provide a fast, visual method to identify which interactions dominate across specific photon energies, helping guide the selection of materials for simulation. When integrated into GEANT4-based workflows, these tools can accelerate the design of radiation shields tailored to the specific mission environments and constraints.

5. CONCLUSIONS

This study presents a comparative visualization framework for gamma-ray shielding materials, transforming theoretical attenuation data into structured insights for material selection across different energy domains. By generating and analyzing dominance plots for photoelectric absorption, Compton scattering, and pair production over a wide photon energy range (1 keV to 20 MeV), the study provides a clearer understanding of how specific materials perform within defined interaction regimes.

Unlike conventional approaches that rely solely on tabulated cross-section values or attenuation coefficients, this method maps interaction mechanisms to energy domains, enabling a systematic comparison of materials and revealing consistent trends governed by atomic number and photon energy. These visuals are particularly valuable for guiding material selection in multilayer or composite shielding systems, where energy-dependent behavior plays a critical role.

A key theoretical insight reaffirmed here is that, under the exponential attenuation model, the overall attenuation of multilayer systems depends on material composition and areal density rather than layer

sequence. However, this conclusion is valid under ideal narrow-beam conditions and does not account for scattered radiation or buildup effects, which may influence shielding performance in practical applications.

Material-specific characteristics play a central role in the observed behavior, with distinct transitions from photoelectric dominance at low energies to Compton scattering at intermediate energies and pair production at higher energies. These systematic trends indicate that effective shielding design must consider energy-dependent interaction mechanisms rather than relying on a single material solution.

While traditional high-Z materials such as lead and tungsten remain highly effective for gamma attenuation, the inclusion of hydrogen-rich materials in shielding configurations is particularly relevant in mixed radiation environments, such as space missions and nuclear facilities, where neutron moderation and secondary radiation control become critical. Therefore, their role should be interpreted within a broader radiation protection context rather than purely gamma-ray attenuation.

The proposed framework serves as a supportive and interpretable tool for preliminary shielding design and material comparison. Nevertheless, the present analysis is based on deterministic cross-section data and does not include secondary radiation processes such as bremsstrahlung, characteristic X-ray emission, or neutron-related interactions, which may become significant in complex shielding environments [54].

Overall, this work provides a systematic and comparative perspective that enhances the interpretability of photon interaction data and supports more informed, application-oriented material selection in radiation shielding studies.

STATEMENT OF PUBLICATION ETHICS

I declare that all processes of the study comply with research and publication ethics, and that I have adhered to ethical rules and principles of scientific citation.

AUTHOR STATEMENT

Ilker Can CELIK: Resources/Materials, Data Collection, Data Processing, Idea/Concept, Design, Supervision/Auditing.

REFERENCES

[1] ICRP, About the ICRP, [Online Resources]. (2025). https://www.icrp.org/page.asp?id=5
[2] International Atomic Energy Agency, Nuclear Data Services, [Online Resources]. (2025). https://www-nds.iaea.org
[3] U.S. Nuclear Regulatory Commission, Materials Regulated by the NRC, [Online Resources]. (2025). https://www.nrc.gov/materials.html
[4] Mkhaiber, A. F., & Dheyaa, A. (2018, May). Experimental study of some shielding parameters for composite shields. In Journal of Physics: Conference Series, 1003 (1), p. 012109. IOP Publishing. https://doi.org/10.1088/1742-6596/1003/1/012109
[5] Levet, A., Kavaz, E., & Özdemir, Y. (2020). An experimental study on the investigation of nuclear radiation shielding characteristics in iron-boron alloys. Journal of Alloys and Compounds, 819, 152946. https://doi.org/10.1016/j.jallcom.2019.152946
[6] Mansy, M. S., Lasheen, Y. F., Breky, M. M., & Selim, Y. (2021). Experimental and theoretical investigation of Pb–Sb alloys as a gamma-radiation shielding material. Radiation Physics and Chemistry, 183, 109416. https://doi.org/10.1016/j.radphyschem.2021.109416.
[7] Sayyed, M. I., Hamad, M. K., Mhareb, M. H. A., Kurtulus, R., Dwaikat, N., Saleh, M., ... & Bradley, D. A. (2022). Assessment of radiation attenuation properties for novel alloys: An experimental approach. Radiation Physics and Chemistry, 200, 110152. https://doi.org/10.1016/j.radphyschem.2022.110152.

[8] Oto, B., Yıldız, N., Akdemir, F., & Kavaz, E. (2015). Investigation of gamma radiation shielding properties of various ores. Progress in Nuclear Energy, 85, 391-403. https://doi.org/10.1016/j.pnucene.2015.07.016.
[9] Hubbell, J.H. & Berger, M.J. (1968). Sec. 4.1: Attenuation Coefficients, Energy Absorption Coefficients, and Related Quantities. and Sec. 4.2: Photon Atomic Cross Sections, in Engineering Compendium on Radiation Shielding, Vol. 1, R.G. Jaeger, ed. (Springer, Berlin), 167-202.
[10] Hubbell, J.H. (1969). Photon Cross Sections, Attenuation Coefficients, and Energy Absorption Coefficients from 10 keV to 100 GeV, NSRDS-NBS 29.
[11] Hubbell, J.H. (1977). Photon Mass Attenuation and Mass Energy-Absorption Coefficients for H, C, N, O, Ar, and Seven Mixtures from 0.1 keV to 20 MeV, Rad. Res., 70, 58-81.
[12] Hubbell, J.H. (1982). Photon Mass Attenuation and Energy-Absorption Coefficients from 1 keV to 20 MeV, Int. J. Appl. Radiat. Isot, 33, 1269-1290.
[13] Hubbell, J.H., Gimm, H.A. & Øverbø, I. (1980). Pair, Triplet, and Total Atomic Cross Sections (and Mass Attenuation Coefficients) for 1 MeV-100 GeV Photons in Elements Z = 1 to 100, J. Phys, Chem. Ref. Data 9, 1023-1147.
[14] Hubbell, J.H., Veigele, W.M.J., Briggs, E.A., Brown, R.T., Cromer, D.T. & Howerton, R.J. (1975). Atomic Form Factors, Incoherent Scattering Functions, and Photon Scattering Cross Sections, J. Phys. Chem. Ref. Data 4, 471-538; erratum in 6, 615-616 (1977).
[15] Saloman, E.B., Hubbell, J.H. & Scofield, J.H. (1988), X-Ray Attenuation Cross Sections for Energies 100 eV to 100 keV and Elements Z = 1 to = 92, At. Data Nucl. Data Tables 38, 1-197.
[16] Saloman, E. B. & Hubbell, J. H. (1987). Critical Analysis of Soft X-ray Cross Section Data, Nucl. Instr. Meth. A255, 38-42.
[17] Saloman, E. B. & Hubbell, J. H. (1986). X-ray Attenuation Coefficients: Comparison of the Experimental Database with Henke and Scofield, NBS Report NBSIR 86-3431.
[18] Berger, R.T. (1961). The X- or Gamma-Ray Energy Absorption or Transfer Coefficient: Tabulations and Discussion, Rad. Res. 15, 1-29.
[19] Seltzer, S.M. (1993). Calculation of Photon Mass Energy-Transfer and Mass Energy-Absorption Coefficients, Rad. Res. 136, 147-170.
[20] Seltzer, S.M. & Hubbell, J.H. (1995). Tables and Graphs of Photon Mass Attenuation Coefficient and Mass Energy-Absorption Coefficients for Photon Energies 1 keV to 20 MeV for Elements Z = 1 to 92 and Some Dosimetric Materials, Appendix to invited plenary lecture by J.H. Hubbell ``45 Years (1950-1995) with X-Ray Interactions and Applications" presented at the 51st National Meeting of the Japanese Society of Radiological Technology, April 14-16, 1995, Nagoya, Japan.
[21] McMaster, W.H., Del Grande, N.K., Mallett, J.H, & Hubbell, J.H. (1969). Compilation of X-ray Cross Sections, Lawrence Livermore Lab., Report UCRL-50174.
[22] Storm, E. & Israel, H.I. (1970). Photon Cross Sections from 1 keV to 100 MeV for Elements Z=1 to Z=100, Nucl. Data Tables A7, 565-681.
[23] Veigele, W.J. (1973). Photon Cross Sections from 0.1 keV to 1 MeV for Elements Z=1 to Z=94, Atomic Data 5, 51-111.
[24] Plechaty, E.F., Cullen, D.E. & Howerton, R.J. (1978). Tables and Graphs of Photon-Interaction Cross Sections from 0.1 keV to 100 MeV Derived from the LLNL Evaluated-Nuclear-Data Library, Lawrence Livermore National Laboratory Report UCRL-5400, Vol. 6, Rev. 2.
[25] Henke, B.L., Lee, P., Tanaka, T.J., Shimabukuro, R.L. & Fujikawa, B.K. (1982). Low Energy X-ray Interaction Coefficients: Photoabsorption, Scattering and Reflection, Atomic Data and Nuclear Data Tables, 27,1-144.
[26] Scofield, J.H. (1973). Theoretical Photoionization Cross Sections from 1 to 1500 keV, Lawrence Livermore Laboratory Report UCRL-51326.
[27] Cullen, D.E., Chen, M.H., Hubbell, J.H., Perkins, S.T., Plechaty, E.F., Rathkopf, J.A. & Scofield, J.H. (1989). Tables and Graphs of Photon-Interaction Cross Sections from 10 eV to 100 GeV Derived from the LLNL Evaluated Photon Data Library (EPDL), Part A: Z = 1 to 50; Part B: Z = 51 to 100, Lawrence Livermore National Laboratory Report UCRL-50400, Vol. 6, Rev. 4.
[28] Higgins, P.D., Attix, F.H., Hubbell, J.H., Seltzer, S.M., Berger, M.J. & Sibata, C.H. (1992). Mass Energy-Transfer and Mass Energy-Absorption Coefficients, Including In-Flight Positron Annihilation for Photon Energies 1 keV to 100 MeV, NISTIR 4812.

[29] Leroux, J, & Thinh, T.P. (1977). Revised Tables of X-ray Mass Attenuation Coefficients, Corporation Scientifique Classique, Quebec.
[30] Tekin, H.O. & Manici, T. (2017). Simulations of mass attenuation coefficients for shielding materials using the MCNP-X code. NUCL SCI TECH, 28, 95. https://doi.org/10.1007/s41365-017-0253-4
[31] Yoriyaz, H., Moralles, M., de Tarso Dalledone Siqueira, P., da Costa Guimarães, C., Belonsi Cintra, F., & Dos Santos, A. (2009). Physical models, cross sections, and numerical approximations used in MCNP and GEANT4 Monte Carlo codes for photon and electron absorbed fraction calculation. Medical physics, 36(11), 5198-5213. https://doi.org/10.1118/1.3242304
[32] Almatari, M., Issa, S. A., Dong, M. G., Sayyed, M. I., & Ayad, R. (2019). Comparison between MCNP5, Geant4 and experimental data for gamma rays attenuation of PbO–BaO–B2O3 glasses. Heliyon, 5(8). https://doi.org/10.1016/j.heliyon.2019.e02364
[33] Ozdogan, H., Kilicoglu, O., Akman, F., & Agar, O. (2022). Comparison of Monte Carlo simulations and theoretical calculations of nuclear shielding characteristics of various borate glasses including Bi, V, Fe, and Cd. Applied Radiation and Isotopes, 189, 110454. https://doi.org/10.1016/j.apradiso.2022.110454
[34] Veigele, W.J. (1973). Photon Cross Sections from 0.1 keV to 1 MeV for Elements Z=1 to Z=94, Atomic Data, 5, 51-111.
[35] NIST, XCOM: Photon Cross Section Database [Online Resources]. (2025). https://physics.nist.gov/PhysRefData/Xcom/Text/intro.html
[36] Berger, M. J., Hubbell, J. H., Seltzer, S. M., Coursey, J. S., & Zucker, D. S. [Online Resources] (1999). XCOM: Photon Cross Section Database, NIST. http://physics.nist.gov/xcom
[37] NIST, X-ray Mass Attenuation Coefficients – Introduction [Online Resources] (2025). https://physics.nist.gov/PhysRefData/XrayMassCoef/intro.html
[38] Hubbell, J. H. & Seltzer, S. M. (1995). X-Ray Mass Attenuation Coefficients – Table 1, National Institute of Standards and Technology https://physics.nist.gov/PhysRefData/XrayMassCoef/tab1.html
[39] Hubbell, J. H. & Seltzer, S. M. (1995). X-Ray Mass Attenuation Coefficients – Table 2, National Institute of Standards and Technology, https://physics.nist.gov/PhysRefData/XrayMassCoef/tab2.html
[40] Tsoulfanidis N. & Landsberger S. (2015). Measurement and Detection of Radiation, 4th Ed. (Taylor & Francis).
[41] Sathish, K. V., Sowmya, N., Munirathnam, R., Manjunatha, H. C., Seenappa, L., & Sridhar, K. N. (2023). Radiation shielding properties of aluminium alloys. Radiation Effects and Defects in Solids, 178(9-10), 1301-1320. https://doi.org/10.1080/10420150.2023.2249180
[42] Sharma, A. K., & Jindal, N. (2026). Investigation of Gamma-Ray Attenuation in Shielding Metals: A Monte Carlo Simulation. In Macromolecular Symposia (p. e70312). https://doi.org/10.1002/masy.70312.
[43] Alsaiari, N. S., Alsufyani, S. J., Alrowaili, Z. A., Eke, C., Sriwunkum, C., & Al-Buriahi, M. S. (2025). Radiation attenuation, dose rate and buildup factors of gallium silicate glass system for nuclear shielding applications. Radiation Physics and Chemistry, 229, 112500. https://doi.org/10.1016/j.radphyschem.2024.112500.
[44] Sathish, K. V., Manjunatha, H. C., Vidya, Y. S., Seenappa, L., Sridhar, K. N., Gupta, P. D., & Raj, A. C. (2022). Gamma, X-ray, and neutron shielding properties of silicon–germanium alloys. Canadian Journal of Physics, 100(12), 543-549. https://doi.org/10.1139/cjp-2021-0080.
[45] Ekinci, N., El-Agawany, F. I., Gurol, A., Rammah, Y. S., Ahmed, E. M., Yılmaz, D., ... & Somer, M. (2022). Physical properties, experimental and theoretical gamma-ray shielding properties of some boron compounds. Radiation Physics and Chemistry, 194, 110012. https://doi.org/10.1016/j.radphyschem.2022.110012.
[46] Sathish, K. V., Manjunatha, H. C., Seenappa, L., Sridhar, K. N., Sowmya, N., & Raj, S. A. C. (2022). Gamma, X-ray and neutron shielding properties of iron boron alloys. Materials Today: Proceedings, 49, 613-619. https://doi.org/10.1016/j.matpr.2021.04.516.
[47] Dipto, R. R., & Mollah, A. S. (2025). Comparative Study on Gamma Radiation Attenuation Parameters between In-House Developed and Locally Available Shielding Materials. International Journal of Chemistry and Chemical Engineering Systems. 10, 1-16.

[48] Aloraini, D. A., Hanfi, M. Y., Sayyed, M. I., Naseer, K. A., Almuqrin, A. H., Tamayo, P., ... & Mahmoud, K. A. (2022). Design and gamma-ray attenuation features of new concrete materials for low-and moderate-photons energy protection applications. Materials, 15(14), 4947. https://doi.org/10.3390/ma15144947.
[49] Yi, C. Y., Kim, Y. H., Kim, I. J., Park, J. I., & Seong, Y. M. (2024). Measurement of average mass attenuation coefficient of air for 137Cs gamma-ray irradiation beam. Metrologia, 61(6), 065005. https://doi.org/10.1088/1681-7575/ad8091.
[50] Mishra, A., & Khanal, R. (2023). Scattering of gamma radiation by air in the ambient environment using gamma ray spectrometry. Kuwait Journal of Science, 50(3B). https://doi.org/10.48129/kjs.17253.
[51] Arif Sazali, M., Alang Md Rashid, N. K., & Hamzah, K. (2019, June). A review on multilayer radiation shielding. In IOP Conference Series: Materials Science and Engineering (Vol. 555, No. 1, p. 012008). IOP Publishing. https://doi.org/10.1088/1757-899X/555/1/012008
[52] Daneshvar, H., Milan, K. G., Sadr, A., Sedighy, S. H., Malekie, S., & Mosayebi, A. (2021). Multilayer radiation shield for satellite electronic components protection. Scientific reports, 11(1), 20657. https://doi.org/10.1038/s41598-021-99739-2
[53] Guan, S., Fu, G., Wan, B., Wang, X., & Chen, Z. (2025). Multi-objective optimization and reliability assessment of multi-layer radiation shielding for deep space missions. Aerospace, 12(4), 337. https://doi.org/10.3390/aerospace12040337
[54] Allison, J. W. (1961). Gamma Radiation Absorption Coefficients of Various Materials Allowing for Bremsstrahlung and Other Secondary Radiations. *Australian Journal of Physics*, *14*(4), 443-468.